PERGAMON

Journal of Structural Geology 22 (2000) 65–79

JOURNAL OF STRUCTURAL GEOLOGY

www.elsevier.nl/locate/jstrugeo

Dislocation creep of fine-grained recrystallized plagioclase under low-temperature conditions

Norio Shigematsu[a,*], Hidemi Tanaka[b]

[a]*Department of Earth Sciences, School of Education, Waseda University, Nishiwaseda, 1-6-1 Shinjuku-ku, Tokyo 169-8050, Japan*
[b]*Department of Earth Sciences, Faculty of Science, Ehime University, Bunkyo 3, Matsuyama, Ehime 790-8577, Japan*

Received 8 July 1998; accepted 11 August 1999

Abstract

Lattice preferred orientation (LPO) and dislocation substructure of fine-grained plagioclase were investigated in ultramylonite from a shear zone along the Hatagawa fault zone in northeast Japan. In the shear zone, the orthoclase mole fraction of the recrystallized alkali-feldspar is not less than 0.94. This composition suggests that deformation occurred below 500°C. Selected area diffraction by transmission electron microscopy (TEM) for an electron-transparent foil and an X-ray texture goniometer (XTG) were used to determine the LPO of plagioclase. Burgers vectors of dislocations were determined by invisibility criteria. The (100), (010), and (001) pole figures reveal strong preferred orientations. The XTG results are consistent with the LPO determined by TEM. The TEM observations confirmed the presence of at least six Burgers vectors. These Burgers vectors or the net slip directions of multiple systems are almost parallel to the lineation. Thus the present study indicates ductility by dislocation creep for fine-grained plagioclase in ultramylonite deformed at relatively low temperature. The LPO pattern and the Burgers vectors determined in this study are different from those of deformation at much higher temperature. Thus the present study also suggests a switching of the slip systems for plagioclase depending on the temperature.

1. Introduction

In deformed rocks under middle to upper crustal conditions, the plastic deformation of feldspar has received little attention, even though this mineral is the dominant phase in the crust. Wet quartzite has been considered to control the plastic strength of the middle to upper crust (e.g. Carter and Tsenn, 1987; Ord and Hobbs, 1989; Handy, 1994). There are some reasons for this. (1) At greenschist facies conditions, feldspar behaves in a brittle manner, and the plastic strength of feldspar has been inferred to be greater than that of quartz (e.g. Simpson, 1985; Vernon and Flood, 1988; Passchier and Trouw, 1996). Thus if quartz is continuous and feldspar is dispersed, quartz will control the rock strength. (2) The strength of feldspar extrapolated from the flow law of Shelton and Tullis (1981) is less than that of wet quartzite (Jaoul et al., 1984; Kronenberg and Tullis, 1984). However this flow law does not represent steady state flow and thus the extrapolation is not valid (Dell'Angelo and Tullis, 1996).

Feldspar commonly develops a clast-matrix structure at low-grade conditions (Passchier and Simpson, 1986; Passchier and Trouw, 1996). The fine feldspathic matrix often extends on both side of a porphyroclast parallel to the mylonite foliation (Allison et al., 1979; Passchier and Simpson, 1986; Passchier and Trouw, 1996), whereas porphyroclasts themselves show abundant evidence of brittle fracturing. This suggests weakness of the fine-grained feldspar.

As a deformation mechanism in fine-grained feldspar, grain boundary sliding has been proposed (Boullier and Gueguen, 1975; Allison et al., 1979; Kerrich et al., 1980; Behrman and Mainprice, 1987; Tullis and Yund, 1991; Fitz Gerald and Stünitz, 1993; Stünitz and Fitz Gerald, 1993; Fliervoet et al., 1997;

* Corresponding author.
E-mail address: snorio@mn.waseda.ac.jp (N. Shigematsu)

0191-8141/00/$ - see front matter
PII: S0191-8141(99)00132-7

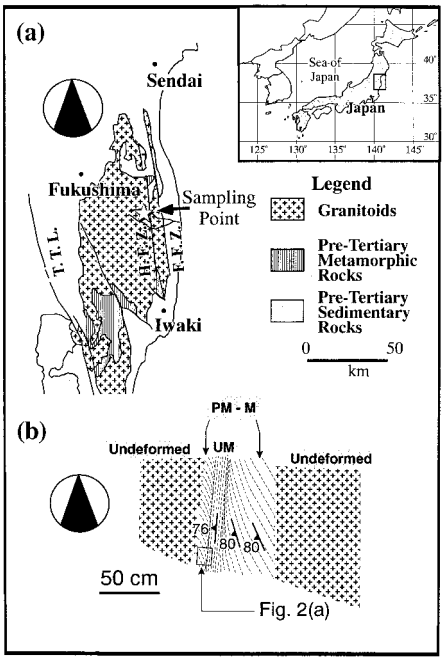

Fig. 1. (a) Location map. H.F.Z = Hatagawa fracture zone. F.F.Z = Futaba fracture zone. T.T.L = Tanakura tectonic line. (b) Sketch map of the outcrop where the sample analyzed in this study was collected. PM, M, UM denote protomylonite, mylonite and ultramylonite parts of the shear zone. The position of Fig. 2(a) is indicated.

Stünitz, 1998). Recrystallization accommodated dislocation creep has also been reported as an important deformation mechanism (Tullis and Yund, 1985, 1987, 1991, 1992; Tullis et. al., 1990; Yund and Tullis, 1991; Dell'Angelo and Tullis, 1996). The size of the fine-grained feldspar, however, is too fine to assess the deformation mechanism by optical means, although the presence of LPO has been ascertained by microscopic observations using a gypsum plate (Tullis and Yund, 1985, 1987). Observation by transmission electron microscopy (TEM) is essential to reveal the deformation mechanism of these grains.

In a shear zone along the Hatagawa fault zone in northeast Japan, TEM observations confirm the grain-size reduction of plagioclase with progressive deformation due to dynamic recrystallization by grain boundary migration (Shigematsu, 1999). In this study, the lattice preferred orientation (LPO) and the dislocation substructure of very fine-grained plagioclase in the shear zone have been investigated, using TEM. To check the result of the LPO by TEM, the preferred orientation of plagioclase has also been measured by an X-ray texture goniometer (XTG).

2. Description of shear zone

Two NNW–SSE trending major faults are exposed at the eastern margin of the Abukuma mountains in northeast Japan. The western and eastern faults are called the Hatagawa and Futaba fault zones, respectively (Watanabe et al., 1953; Sendo, 1958) (Fig. 1). The Hatagawa fault zone has been considered to separate the Southern Kitakami belt from the Abukuma belt (Kubo and Yamamoto, 1990; Otsuki and Ehiro, 1992).

In the study area, the Hatagawa fault zone forms a cataclasite zone about 50 m in width. Granitoids on the eastern side of the Hatagawa fault zone consist of the Kunimiyama granodiorite, the Hachijoishiyama granite, and the Kawabusa granodiorite (Kubo and Yamamoto, 1990). They exhibit mylonite microstructures in which asymmetric microstructures indicate a sinistral sense of shear (Koshiya, 1988).

Small ductile shear zones are locally and sporadically developed in the granitoids on the western side of the Hatagawa fault zone. The widths of these shear zones range from a few millimeters to a few meters. Except for these shear zones the granitoids do not show any features of ductile deformation. These small shear zones together form a NNW–SSE trending zone of about 1 km width, 1 km west of the Hatagawa fault zone. The ductile shear zones form a conjugate set. One of the sets has a NNE–SSW to NE–SW orientation with a dextral sense of shear, and the other has an EW to ESE–WNW orientation with a sinistral sense of shear, indicating that the maximum principal stress direction was oriented almost E–W. Pseudotachylyte has been reported from one of the shear zones (Kubo and Takagi, 1997).

The sample analyzed in this study was collected from one of the outcrops of small-scale shear zones on the western side of the Hatagawa fault zone (Fig. 1), which is the same as in Shigematsu (1999). Sigmoidal foliations are developed along a narrow (70 cm) shear zone (Fig. 2a), indicating a dextral sense of shear. The central part of the shear zone is composed of ultramylonite of 10-cm width, and the deformation becomes stronger toward this ultramylonite zone (Fig. 2b). In the ultramylonite zone, the foliation strikes N6°E and dips 76°W, and the lineation plunges by 8° toward N5°E. Analyses were carried out for the very fine-grained plagioclase in the ultramylonite zone.

3. Analytical procedures

For the analysis of fine-grained plagioclase in ultramylonite, microstructural studies were first undertaken. Following these studies, the LPO and the slip vectors of fine-grained plagioclase were determined by TEM. The LPO were also examined by XTG to check whether the LPO determined by TEM is representative or not. TEM analyses were carried out on a JEOL

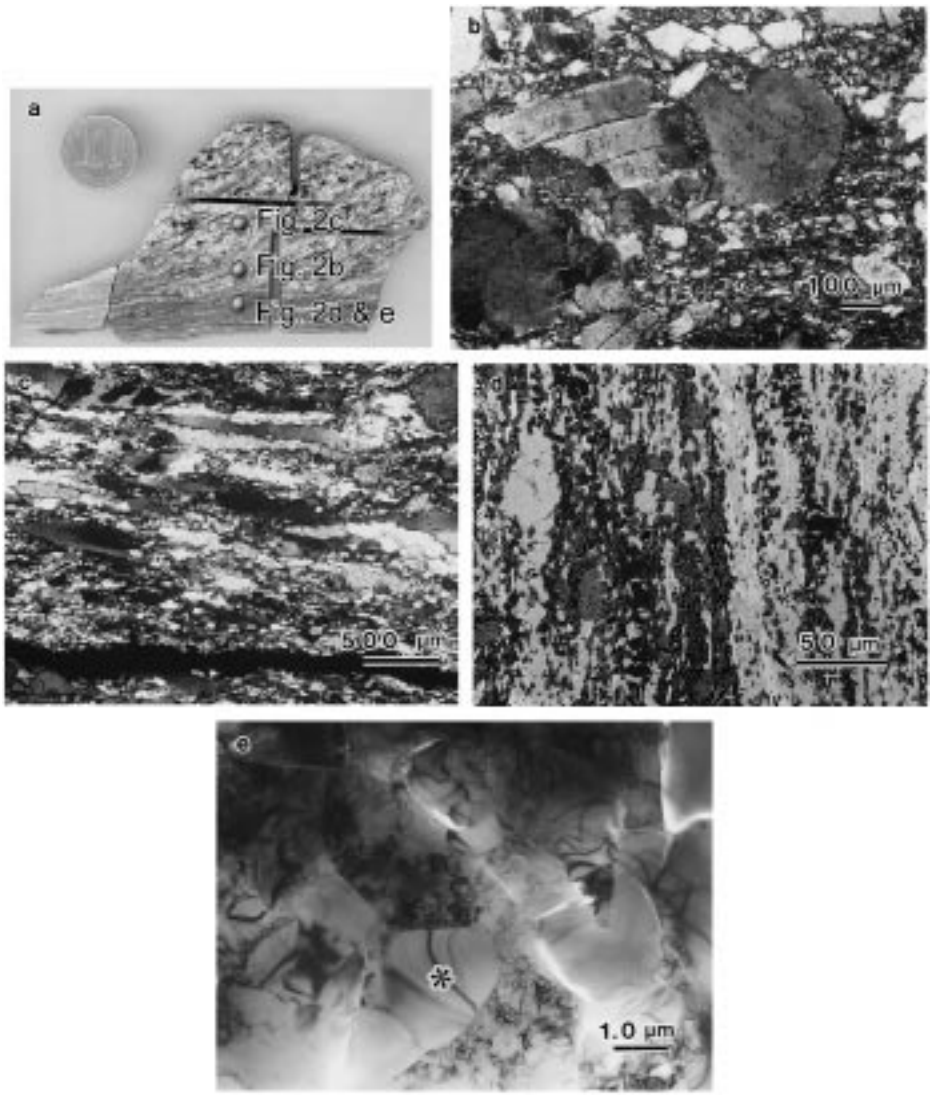

Fig. 2. (a) Sample of the shear zone. The positions of (b), (c), (d) and (e) are indicated. (b) Plagioclase porphyroclast in the moderately deformed part of the shear zone. (c) Quartz in the moderately deformed part of the shear zone. (d) Back-scattered electron image (BEI) of the central part of the shear zone. Contrasts in BEI allow one to visualize K-feldspar (whitish gray), plagioclase (medium gray), and quartz (dark gray). The base of the photograph is subperpendicular to the shear zone orientation. (e) The microstructures of fine-grained plagioclase matrix in the ultramylonite. Diffraction patterns of these grains indicate that almost all of the grains are plagioclase. The grain with asterisk (Grain I-4 in Fig. 4a) has low dislocation density and seems to be growing into the surrounding plagioclase with high dislocation density.

JEM2000FX at Geological Institute, University of Tokyo, operating at 200 kV. A double-tilting goniometer stage was used in all cases. XTG analyses were carried out on a RIGAKU Rint 2000 at Department of Earth Sciences, Ehime University, using Cu $K\alpha_1$ (1.54005 Å) operating at 40 kV and 40 mA.

One electron-transparent foil of selected areas from the thin section from the ultramylonite was prepared by ion-beam thinning. The foil plane was parallel to the lineation and perpendicular to the foliation. After thinning, the specimens were coated with a thin carbon layer to eliminate sample charging during observation.

3.1. LPO determined by TEM

The LPO of feldspar in deformed rocks has been determined previously by U-stage methods (Jensen and Starkey, 1985; Olsen and Kohlstedt, 1985; Kruhl, 1987; Ji and Mainprice, 1988, 1990; Ji et al., 1988, 1994), neutron diffraction techniques (Wenk et al., 1986; Wenk and Pannetier, 1990), and selected area diffraction (SAD) by TEM (Fitz Gerald et al., 1983). Attempts to use conventional X-ray diffraction techniques have failed due to the large number of overlapping diffraction peaks (Wenk et al., 1986; Ji et al., 1994). For the ultramylonite, the grain size of plagio-

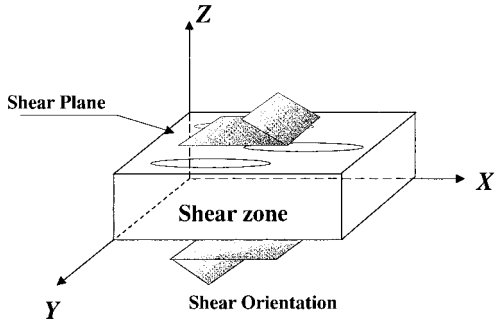

Fig. 3. Sample coordinate system. The coordinate system is defined as Z being perpendicular to the shear zone orientation, Y lying within the shear zone orientation and being perpendicular to the lineation, and X being parallel to lineation and perpendicular to both Y and Z.

clase ranges from a few hundred nanometers to a few micrometers, which is too fine to be measured by U-stage, but can be measured by the SAD technique by TEM. Furthermore TEM can provide unique information on the crystallographic orientation and the correlation between the defect structure induced by deformation and the LPO.

The grain orientation measurements involved tilting the specimen so that a low index zone axis was parallel to the electron beam; the diffraction pattern and tilt angles were recorded (Wenk, 1985; McLaren, 1991). Because of the low symmetry of the plagioclase, two zone axes must be measured to uniquely determine the orientation of an individual grain. The orientation of the zone axis can be determined by indexing the selected area diffraction pattern. For indexing, 20 theoretical patterns for $C\bar{1}$ plagioclase were simulated by the software Mac Tempus.

Each of the two diffraction patterns contains two independent reciprocal lattice vectors, $\mathbf{g}_1$ and $\mathbf{g}_2$ for one diffraction pattern, and $\mathbf{g}_3$ and $\mathbf{g}_4$ for the other diffraction pattern. The reciprocal lattice vectors can also be given in the following form as

$$\mathbf{g}_1 = h_1\mathbf{a}^* + k_1\mathbf{b}^* + l_1\mathbf{c}^* \quad (1a)$$

$$\mathbf{g}_2 = h_2\mathbf{a}^* + k_2\mathbf{b}^* + l_2\mathbf{c}^* \quad (1b)$$

$$\mathbf{g}_3 = h_3\mathbf{a}^* + k_3\mathbf{b}^* + l_3\mathbf{c}^* \quad (1c)$$

$$\mathbf{g}_4 = h_4\mathbf{a}^* + k_4\mathbf{b}^* + l_4\mathbf{c}^* \quad (1d)$$

where $\mathbf{a}^*$, $\mathbf{b}^*$, $\mathbf{c}^*$ are the reciprocal lattice vectors defining the unit cell in the reciprocal space and $h_nk_nl_n$ are the Miller indices of the reflecting planes corresponding to the reciprocal lattice points specified by $\mathbf{g}_n$. Because the specimen was tilted in a crystallographic plane, two of four equations in Eq. (1) are the same. Thus the grain orientation with respect to the sample reference frame (Fig. 3) can be obtained by solving Eq. (1). The orthogonal sample coordinate system is defined with the Z axis perpendicular to the shear zone, the Y axis lying within the shear zone and perpendicular to the lineation, and the X axis perpendicular to both Y and Z (Fig. 3).

To check the accuracy of this method, the reproducibility was examined when five choices of two zone axes were made for one grain. The difference between the choices is in the range of $\pm 5^\circ$. Thus the error due to the tilting of the holder and the choice of the two zone axes is not significantly large. To avoid measurement errors, the specimen was not removed from the double-tilt holder during the grain orientation measurements. This is the reason why only one electron-transparent foil from the ultramylonite was used for the grain orientation measurements.

3.2. Determination of the slip systems

For some grains, the Burgers vector $\mathbf{b}$ was also determined by the invisibility criterion (McLaren, 1991), which strictly applies only to elastically isotropic materials. If the Burgers vector $\mathbf{b}$ satisfies the following condition, the dislocation will be invisible.

$$\mathbf{g} \cdot \mathbf{b} = 0 \quad (2a)$$

for screw dislocation and

$$\mathbf{g} \cdot \mathbf{b} = 0 \quad (2b)$$

and

$$\mathbf{g} \cdot (\mathbf{b} \times \mathbf{u}) = 0 \quad (2c)$$

for edge dislocation, where $\mathbf{g}$ is the diffraction vector and $\mathbf{u}$ is a unit vector parallel to the dislocation line, respectively. However, plagioclase is elastically anisotropic, and a weak contrast is expected in cases where invisibility criteria are satisfied. The determination of slip systems strictly requires the use of the computer image simulation technique (Olsen and Kohlstedt, 1984; Montardi and Mainprice, 1987). In this study, the much simpler approach of 'effective invisibility' was used, and the only characterizations of Burgers vectors were carried out by this method.

3.3. X-ray texture goniometry

The grain orientation measurements by TEM were carried out for one foil from the ultramylonite. There is a difficulty in ascertaining that LPOs determined using this technique are representative for a large volume, thus pole figures were also measured by XTG. In the present investigation, a sample of ultramylonite was first investigated by X-ray powder diffraction to ascertain that patterns could be indexed and phases

were identified. The analysis was performed under the conditions with X-ray sampling with 0.002°, scanning speed 1.0° min^{-1}, divergence slit 1.0°, scattering slit 1.0°, and receiving slit 0.30 mm. Subsequently a pole figure of a uniquely determined plagioclase peak was measured.

For the measurement of the pole figure, two disks with 4.4-cm diameter and 0.0105-cm thickness were prepared, parallel to the shear zone (*XY* plane). Thus this method allows the measurement for larger volumes. The linear absorption coefficients of the sample are 106 and 116 cm^{-1} for Cu $K\alpha$ X-rays, respectively. The pole figures were measured by the transmission method from the pole distance 0.0 to 30.0°, and by the reflection method from the pole distance 25 to 90°. Divergence slit 0.1 mm, scattering slit 4 mm, and receiving slit 3 mm were used for measurement by the transmission method. Divergence slit 1/2°, scattering slit 4 mm, and receiving slit 3 mm were used for measurement by the reflection method.

4. Microstructures and microtextures

4.1. Microstructures

The sample in this study is mainly composed of quartz, plagioclase, K-feldspar, hornblende, and biotite. Rare allanite occurs as accessory phase. Mineral composition does not significantly change during progressive deformation in the shear zone. The anorthite mole fraction of fine-grained plagioclase ranges from

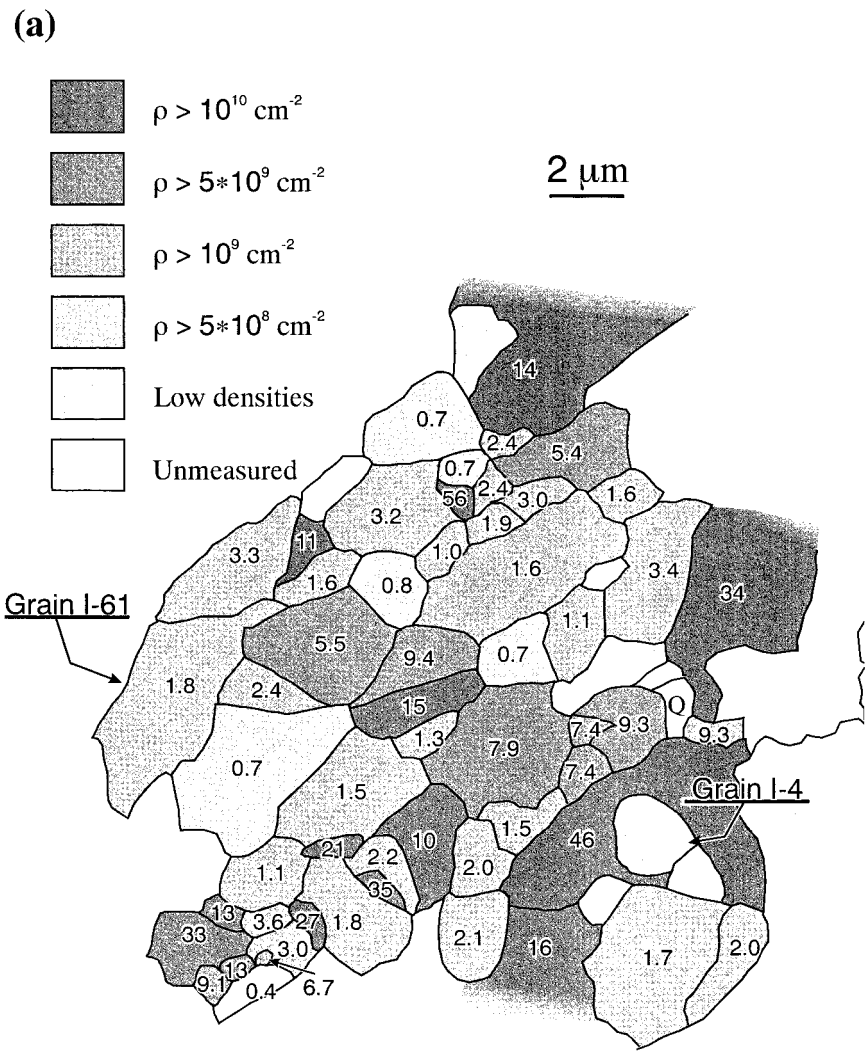

Fig. 4. Microstructural features of the aggregates of fine-grained plagioclase. (a) Line drawings and maps of the dislocation densities in domain I. (b) Line drawings and maps of the dislocation densities in domain II. The grains denoted by (Q) are quartz, hatched areas indicate pores in a foil and the other grains are plagioclase. The numbers in the plagioclase grains indicate the dislocation densities, with units of 10^9 cm^{-2}. The area of Fig. 2(e) corresponds to the domain I.

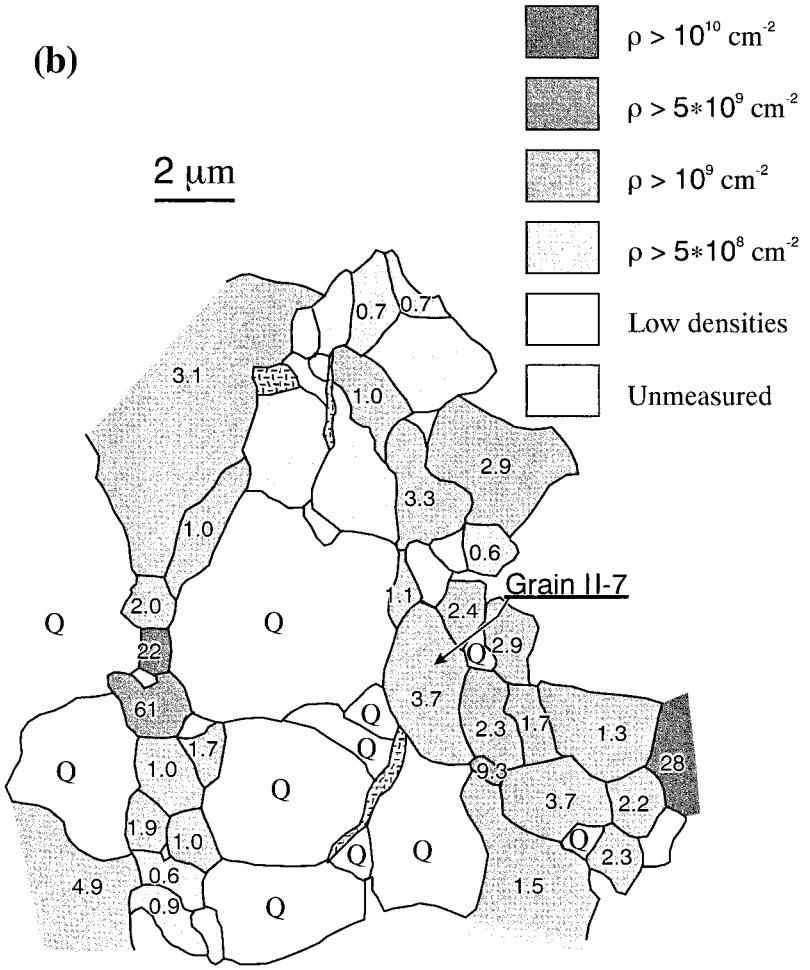

Fig. 4 (*continued*)

0.17 to 0.26; the orthoclase mole fraction of the fine-grained alkali-feldspar ranges from 0.94 to 0.99. The anorthite mole fraction of the core region of plagioclase porphyroclasts ranges from 0.21 to 0.45, whereas that of the rim of plagioclase porphyroclasts is almost the same as that of fine-grained plagioclase (Shigematsu, 1999).

In the moderately deformed part of the shear zone, feldspar develops a clast and matrix structure (Fig. 2b). Porphyroclasts show evidence of brittle fracturing and undulatory extinction, whereas fine-grained matrices extend parallel to the shape fabric in the mylonite. Quartz grains show a core and mantle structure (White, 1976) in which coarse ribbon grains (diameters > 50 μm) are surrounded by fine equant grains (diameters < 50 μm). The coarse ribbon grains have aspect ratios up to 15:1, and their long axes are approximately parallel to the foliation. They exhibit a sweeping undulatory extinction, and commonly contain subgrains (Fig. 2c) (Shigematsu, 1999).

In the central part of the shear zone, feldspar porphyroclasts are rare, and all are smaller than a few tens of micrometers. The fine-grained feldspar matrix shows development of fluxion structures defined by the aligned or elongated clusters of plagioclase and K-feldspar (Fig. 2d). Quartz occurs as elongated clusters of equant grains with diameters less than 50 μm.

In this study, two domains of the fine-grained plagioclase in the ultramylonite from the same TEM foils were analyzed: domain I and domain II. These two domains are separated by a quartz domain. Line drawings and dislocation density maps for both domains are shown in Fig. 4(a) and (b). Domain I consists only of the fine-grained plagioclase, whereas domain II consists both of the fine-grained plagioclase and quartz. In domain II plagioclase occurs as thin layers of fine grains among quartz grains (Fig. 4b). Individual plagioclase grains are equiaxial and range in size from 0.3 to 6.3 μm with an average of 1.54 μm, which is smaller than that of quartz (18.3 μm).

Fine-grained plagioclase in both domains has a variable dislocation density (Figs. 2e and 4). Some grains

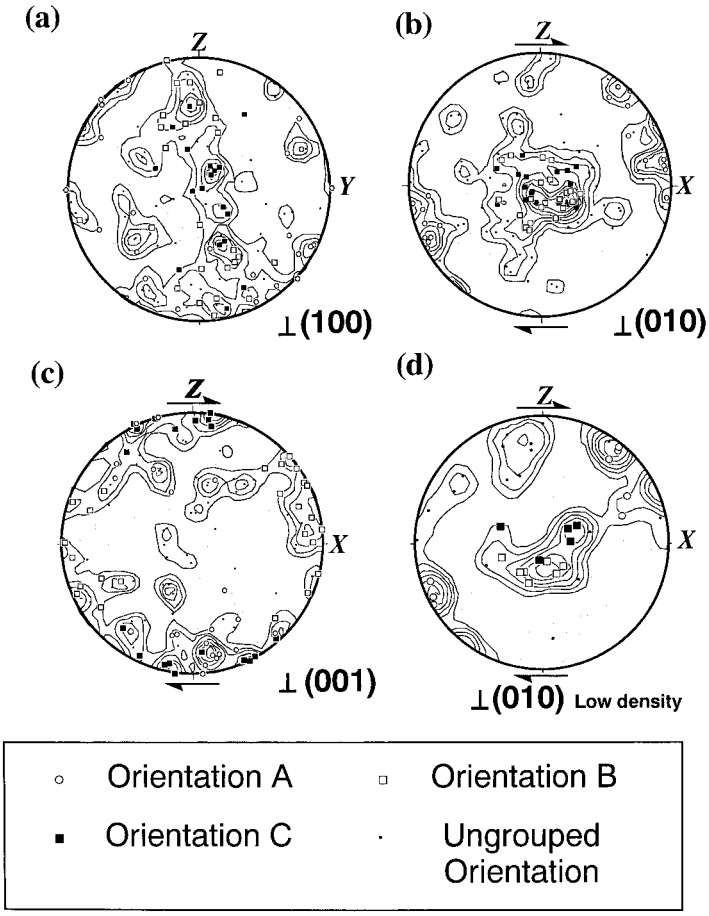

Fig. 5. Pole figures of the fine-grained plagioclase in ultramylonite for (a) (100) plane, (b) (010) plane, (c) (001) plane. (d) The (010) pole figure of low dislocation density grains (dislocation density less than 10^9 cm^{-2}). The *YZ* plane is parallel to the page for (a). The *XZ* plane is parallel to the page for (b), (c), and (d). Equal-area projection, lower-hemisphere, 130 measurements for (a), (b), and (c). Equal-area projection, lower-hemisphere, 38 measurements for (c). Contour intervals for all pole figures: 1.0, 1.5, 2.0, ... , 5.5 times uniform distribution.

have a very low dislocation density ($< 10^8$ cm^{-2}) while others have an intermediate to very high density ($> 10^{10}$ cm^{-2}). The detailed dislocation substructures will be described later. In aggregates of the fine-grained plagioclase, some grains with low dislocation density seem to be growing into adjacent grains with high dislocation density (Fig. 2e).

4.2. LPO determined by TEM

The results of the TEM analyses of LPO of the fine-grained plagioclase are shown in Fig. 5. Fifty-seven grains were measured in domain I, and 73 grains were measured in domain II.

The pole figures of (100), (010), and (001) reveal a preferred orientation (Fig. 5). The (100) pole figure consists of a single girdle, which is oriented at approximately 20° to the specimen *XZ* plane and contains the *X* direction (Fig. 5a). The (010) pole figure consists of two point maxima within a single girdle (Fig. 5b). This single girdle is almost parallel to the foliation, oriented at approximately 20° to the specimen *XY* plane and contains the *Y* direction. The (001) pole figure consists of two point maxima within a single girdle, which is almost parallel to the specimen *XZ* plane (Fig. 5c). One of the point maxima is almost parallel to the specimen *Z*, and the other is oriented at approximately 20° to the *X* direction.

The orientation of half of the grains in Fig. 5 can be classified into three orientation groups, *A*, *B*, and *C*, by considering the (010) and (001) orientations. For orientation *A* (open circle in Fig. 5), the pole of the (010) plane is oriented at approximately 20° to the *X* direction of the sample coordinate system and the (001) plane is almost parallel to the *XY* plane. For orientation *B* (open square in Fig. 5), the pole of the (010) plane is approximately parallel to the *Y* direction and the pole of the (001) plane is oriented at approximately 20° to the *X* direction. For orientation *C* (solid square in Fig. 5), the pole of the (010) plane is approximately parallel to the *Y* direction and the (001) plane is almost parallel to the *XY* plane. The grains

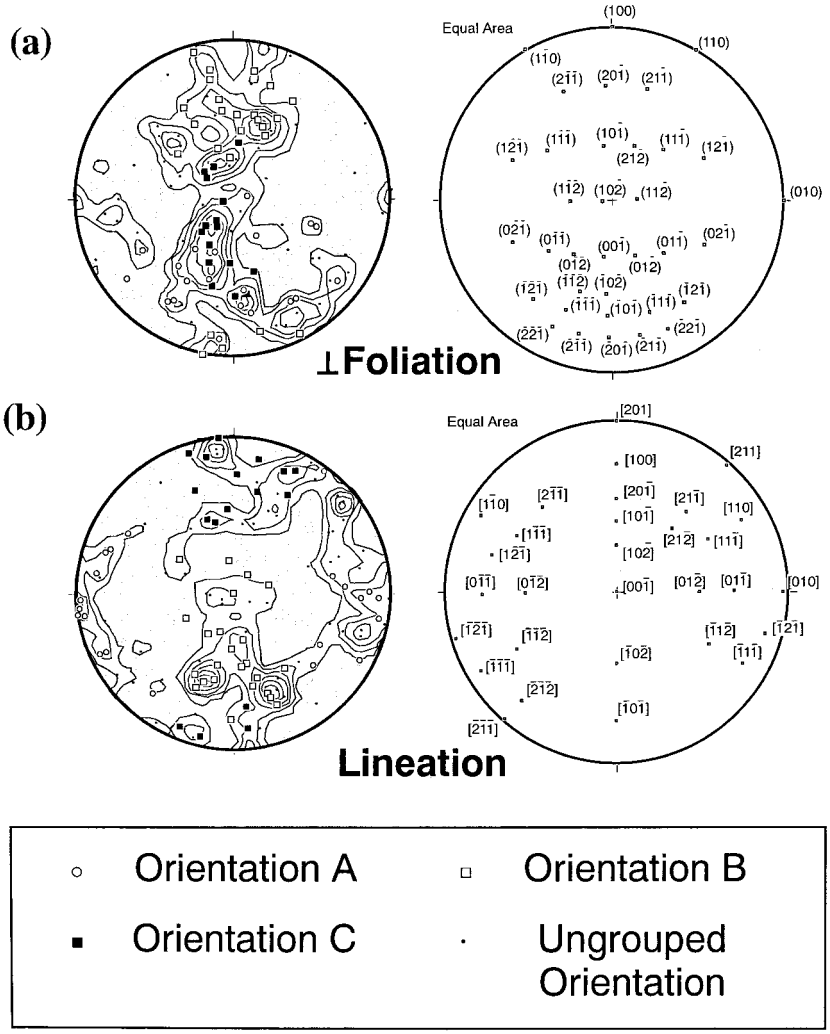

Fig. 6. Inverse pole figures of (a) the foliation pole and (b) the lineation. Equal-area projection lower hemisphere, 130 measurements. Contour intervals for all pole figures: 1.0, 1.5, 2.0, ... , 3.5 times uniform distribution. Note the separation of the orientation groups in the inverse pole figure of the lineation.

which belong to none of the orientation groups *A*, *B*, or *C* (small dots in Fig. 5) have rather weak LPO compared with the grains which do belong.

Figure 5(d) shows the (010) pole figure of low dislocation density grains (dislocation density less than 10^9 cm^{-2}). This LPO pattern is almost the same as that of all grains (Fig. 5b), although it is weaker. The ratio of orientation groups *A*, *B*, and *C*, and ungrouped grains is also similar to that for all grains.

The probability of finding a particular crystal direction aligned with a given specimen direction is expressed in the form of inverse pole figures in Fig. 6. The foliation pole is aligned in directions which are almost perpendicular to [010], such as the poles to $(10\bar{1})$, $(11\bar{1})$, (001), $(1\bar{1}1)$, and $(01\bar{1})$ (Fig. 6a). The foliation pole of orientation *B* is aligned in directions close to the poles to $(10\bar{1})$, $(11\bar{1})$, and (100), whereas the foliation poles of orientations *A* and *C* are aligned in directions close to the poles to (001), (101), (111), and $(1\bar{1}1)$ (Fig. 6a).

The lineation is seen to be aligned in directions either close to [010] or on (010) plane, such as [110], $[11\bar{1}]$, $[01\bar{1}]$, $[1\bar{1}2]$ and $[1\bar{1}1]$, or [101], [001] and [100] (Fig. 6b). The inverse pole figures of the lineation clearly separate the alignments of the orientation groups *A*, *B*, and *C*. The lineation of orientation *A* is aligned in directions close to [010]. The lineation of orientation *B* is aligned in directions close to [001] and [101]. The lineation of orientation *C* is aligned in directions close to [100] and [101].

4.3. X-ray texture goniometry

The X-ray 2θ profile of powder is shown in Fig. 7(a). Most of the peaks of plagioclase are overlapped with other peaks of plagioclase or peaks of other min-

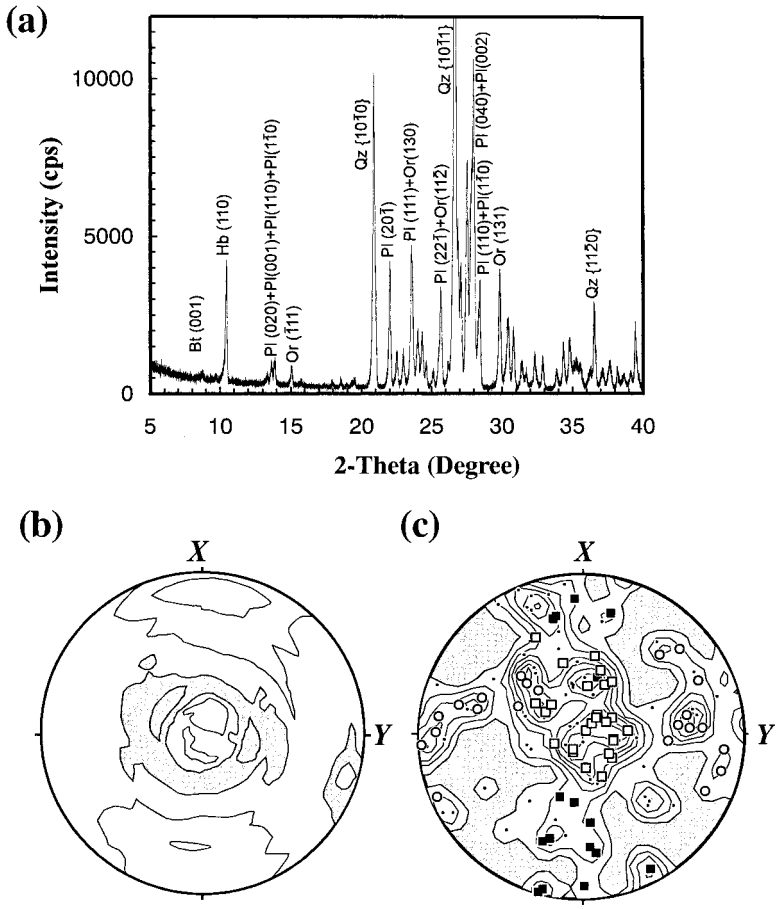

Fig. 7. Comparison between the pole figures measured by TEM and X-ray texture goniometory. (a) The X-ray 2θ profile of powder. Bt: biotite; Qz: quartz; Hb: Hornblende; Pl: Plagioclase; Or: Orthoclase. (b) The $(20\bar{1})$ pole figure measured by XTG. Equal-angle projection, lower-hemisphere. Contour intervals for the figure: 0.72, 0.90, 1.08, and 1.26 times normalized intensity. Shaded area indicates the intensity is weaker than 0.9 times normalized intensity. (c) The $(20\bar{1})$ pole figure measured by TEM. Equal-angle projection, lower-hemisphere, 130 measurements. Contour intervals for the figure: 0.5, 1.0, 1.5, ... , 3.5 times uniform distribution. Open circle is group *A*, open square is group *B*, solid square is group *C*, and small solid circle is the other orientations.

erals. A peak at $2\theta = 22.01^\circ$ was used for the measurement of the pole figures. This peak corresponds to the overlapped peak of plagioclase $(20\bar{1})$ and biotite (111). Because the intensity of the biotite peak at $2\theta = 8.75^\circ$ [biotite (001)] is weak in the powder diffraction, it is interpreted that the peak at $2\theta = 22.01^\circ$ mainly comes from the reflection by plagioclase $(20\bar{1})$.

The $(20\bar{1})$ pole figure by XTG from one sample displays an LPO and consists of a single girdle that contains the specimen *XZ* plane with a maximum in the specimen *X* direction (Fig. 7b). Almost the same pattern was obtained from the other sample. The concentration around the specimen *X* direction has a broad angle. The $(20\bar{1})$ pole figure by TEM is also shown in Fig. 7(c) for comparison. Both of the pole figures (Fig. 7b and c) contain a single girdle parallel to the specimen *XZ* plane, although they are not quite the same. Therefore, it was interpreted that the XTG results are consistent with the LPO determined by TEM, and the LPO by TEM is representative of a large volume.

4.4. Determination of Burgers vector

For the determination of Burgers vector **b**, three grains were selected, grain I-61 from domain I (Fig. 4a), grains II-7 and II-51 from domain II (Fig. 4b). Half of the grains can be classified into three orientation groups, *A*, *B*, and *C*. The selected grains I-61, II-7, and II-51 have orientation *A*, intermediate orientation of *B* and *C*, and orientation *B*, respectively.

The substructures in grain I-61 are illustrated in Fig. 8. Dislocations parallel to the short side of the micrographs are in strong contrast for $\mathbf{g} = (040)$ (Fig. 8a), whereas these are out of contrast for $\mathbf{g} = (001)$ (Fig. 8b). These dislocations are also out of contrast for $\mathbf{g} = (\bar{1}12)$ (Fig. 8c). Therefore these dislocations are screw dislocations with $\mathbf{b} = 1/2[110]$, possibly with slip system $(001)1/2[110]$ by considering the previously determined slip systems (Gandais and Williaime, 1984).

The substructures in grain II-7 are illustrated in Fig. 9. In the micrograph under the reflection $\mathbf{g} = (002)$

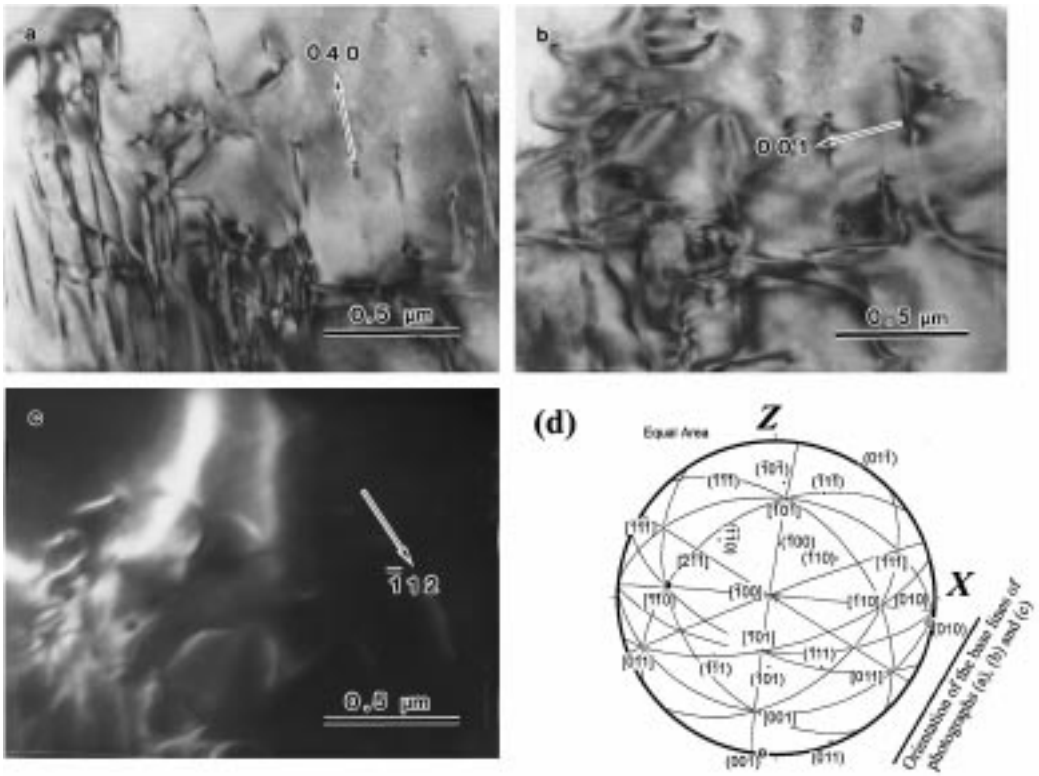

Fig. 8. Substructures in the grain I-61. Bright field images under the reflections (a) $\mathbf{g} = (040)$, (b) $\mathbf{g} = (001)$. Dark field image under the reflection (c) $\mathbf{g} = (\bar{1}12)$. (d) Crystallographic orientation of grain I-61 which corresponds to orientation *A*. Scale bars = 0.5 μm.

(Fig. 9a), an array of dislocations forming a low-angle sub-grain boundary can be seen. This microstructure suggests glide and the climb of the dislocations. This sub-grain boundary is out of contrast for $\mathbf{g} = (200)$ (Fig. 9b) $\mathbf{g} = (022)$ and $\mathbf{g} = (\bar{1}11)$. Therefore the Burgers vector of these dislocations is $\mathbf{b} = 1/2[01\bar{1}]$. Most of the dislocations are in strong contrast for $\mathbf{g} = (20\bar{2})$ which satisfies Eq. (2a) for $\mathbf{b} = [101]$, although the [101] of grain II-7 is almost parallel to the lineation of the sample (Fig. 9c). This indicates that the $\mathbf{b} = [101]$ is uncommon in this grain. TEM observations also confirm the presence of $\mathbf{b} = [001]$ and [100] in the grain II-7 (Fig. 9d). Some unidentified dislocations are out of contrast only for $\mathbf{g} = (\bar{1}11)$ (Fig. 9d). The possible Burgers vectors for these dislocations are $\mathbf{b} = 1/2[211]$, or $1/2[11\bar{2}]$, which satisfies $\mathbf{g} \cdot \mathbf{b} = 0$ for $\mathbf{g} = (\bar{1}11)$. These dislocations are in strong contrast for $\mathbf{g} = (20\bar{1})$, suggesting $\mathbf{b} = 1/2[211]$ which is found in grain II-51.

The substructures in grain II-51 are illustrated in Fig. 10. A line drawing of the dislocations in grain II-51 and the determined Burgers vectors is given in Fig. 10(c). The contrast analyses confirm the presence of the $\mathbf{b} = 1/2[211]$, $1/2[1\bar{1}2]$, and $1/2[11\bar{2}]$ in grain II-51 (Fig. 10c). Although [101] of grain II-51 is almost parallel to the lineation (Fig. 10b), contrast analysis reveals a lack of dislocations with $\mathbf{b} = [101]$.

TEM observations confirmed the presence of $\mathbf{b} = 1/2[110]$ from grain I-61, and $1/2[01\bar{1}]$, [001], and [100] from grain II-7, $1/2[1\bar{1}2]$ and $1/2[11\bar{2}]$ from grain II-51. These Burgers vectors were also confirmed in other grains. Some other dislocations are out of contrast only for one diffraction condition, indicating Burger's vectors not in the list above. Therefore at least six Burger's vectors exist in fine-grained plagioclase in ultramylonite. The dislocation segments tend to be very straight and parallel to crystallographic orientations, and some dislocation tangles were observed. These observations suggest that dislocation climb is not a common process in deformation, although a few subgrain boundaries were observed.

5. Discussion

5.1. Deformation mechanisms of fine-grained plagioclase

The present study provides some constraints on the deformation mechanism of fine-grained plagioclase in the ultramylonite. LPO analyses of the fine-grained plagioclase reveal a strong preferred orientation (Figs. 5 and 6), suggesting dislocation creep. Half of the grains can be classified into three orientation groups, *A*, *B*, and *C*. The inverse pole figures of the lineation (Fig. 6b) clearly separate the alignments of the orientation groups, suggesting each orientation group is

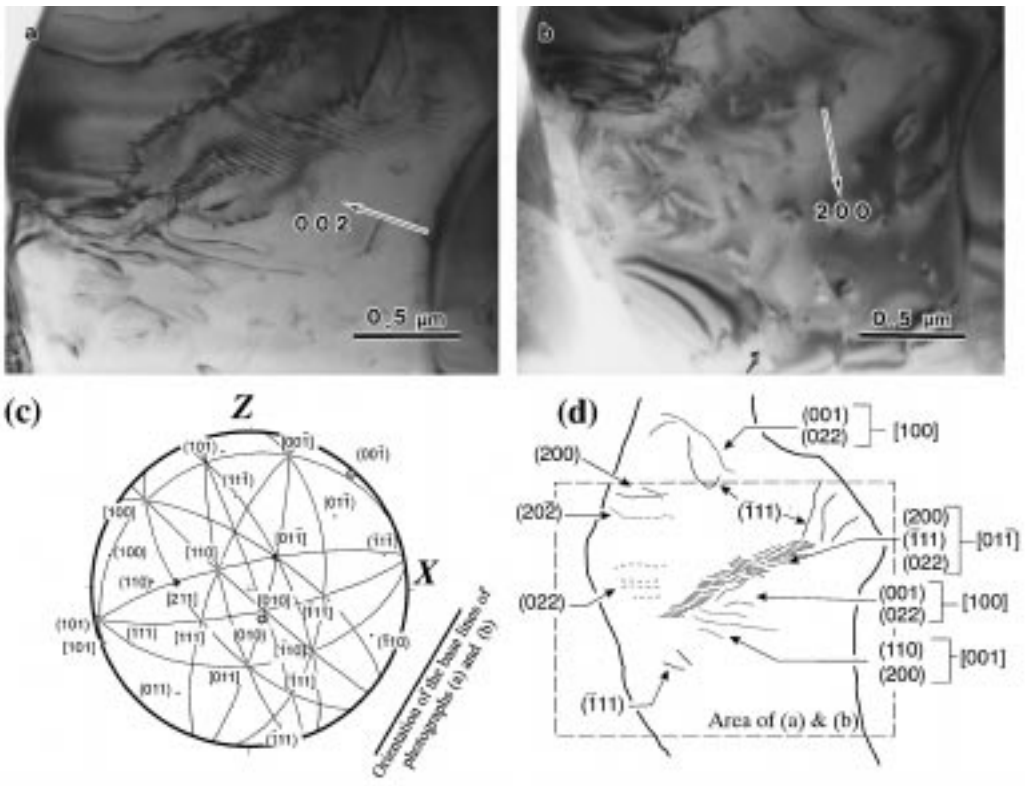

Fig. 9. Substructures in grain II-7. TEM micrographs are taken under the reflections (a) $\mathbf{g} = (002)$ and (b) $\mathbf{g} = (200)$. (c) Crystallographic orientation of grain II-7 which corresponds to orientation of intermediate between groups *B* and *C*. (d) Line drawing of the dislocations in grain II-7. Diffraction conditions are shown for which the arrowed dislocations are out of contrast indicated by two or more reflective planes, e.g. (022). Burgers vectors consistent with this invisibility are also shown. Dislocations without any constraints are not shown.

controlled by the dislocations with different slip vectors. Therefore consistency between the orientation groups and the determined Burgers vectors is expected.

In grain I-61 which has orientation *A*, the determined Burgers vector $\mathbf{b} = 1/2[110]$ is aligned with the orientation close to the lineation (Fig. 8), suggesting that the orientation *A* is mainly controlled by the slip with $\mathbf{b} = 1/2[110]$. Grain II-7 has an intermediate orientation between *B* and *C*. The contrast analysis reveals dislocations with $\mathbf{b} = 1/2[01\bar{1}]$ and $1/2[211]$ as dominant slip vectors (Fig. 9). The simultaneous activity of these slip vectors can yield a net slip direction parallel to [101] which is close to the lineation, i.e. $1/2[211] - 1/2[01\bar{1}] = [101]$. In grain II-51 which has orientation *B*, the simultaneous activity of determined slip vectors, $\mathbf{b} = 1/2[211]$, $1/2[1\bar{1}2]$, and $1/2[11\bar{2}]$ (Fig. 10d) can yield a net slip direction parallel to the [101] axis which is close to the lineation, i.e. $[211] + [1\bar{1}2] = 3[101]$. It is inferred that the net slip directions of the multiple systems mainly control the orientations *B* and *C*. Therefore, consistency of the orientation groups with the determined Burgers vectors was found. However, the significance of this conclusion depends upon the Burgers vector determination for the visible dislocations, and image simulation will be necessary for more detailed discussion.

The fine plagioclase grains in the ultramylonite have a variable dislocation density (Fig. 4) and some grains with low dislocation density seem to be growing into adjacent grains with high dislocation density (Fig. 2d). This microstructure is the same as that of recrystallization-accommodated dislocation creep as reported in experimentally deformed plagioclase (Tullis and Yund, 1985; 1987; 1991; 1992; Tullis et al., 1990; Yund and Tullis, 1991) and low stacking fault energy metals (e.g. Sakai and Jonas, 1984; Sakai et al., 1986). Therefore the observations in this study strongly suggest recrystallization-accommodated dislocation creep of the fine-grained plagioclase.

The effect of grain boundary migration on LPO development could indeed be important under particular conditions (e.g. Gleason et al., 1993). However, the LPO of the low dislocation density grains is similar to that of all grains (Fig. 5b and d). This suggests that the effect of grain boundary migration on LPO is not so large (host grain control), or the grain boundary migration favors the survival of grains with slip system orientation for easy glide (Herwegh and Handy, 1996). In either case, grain boundary migration produces soft oriented grains. Moreover, the accumulated dislocations are continuously destroyed by grain boundary migration. Thus this process operated as an important

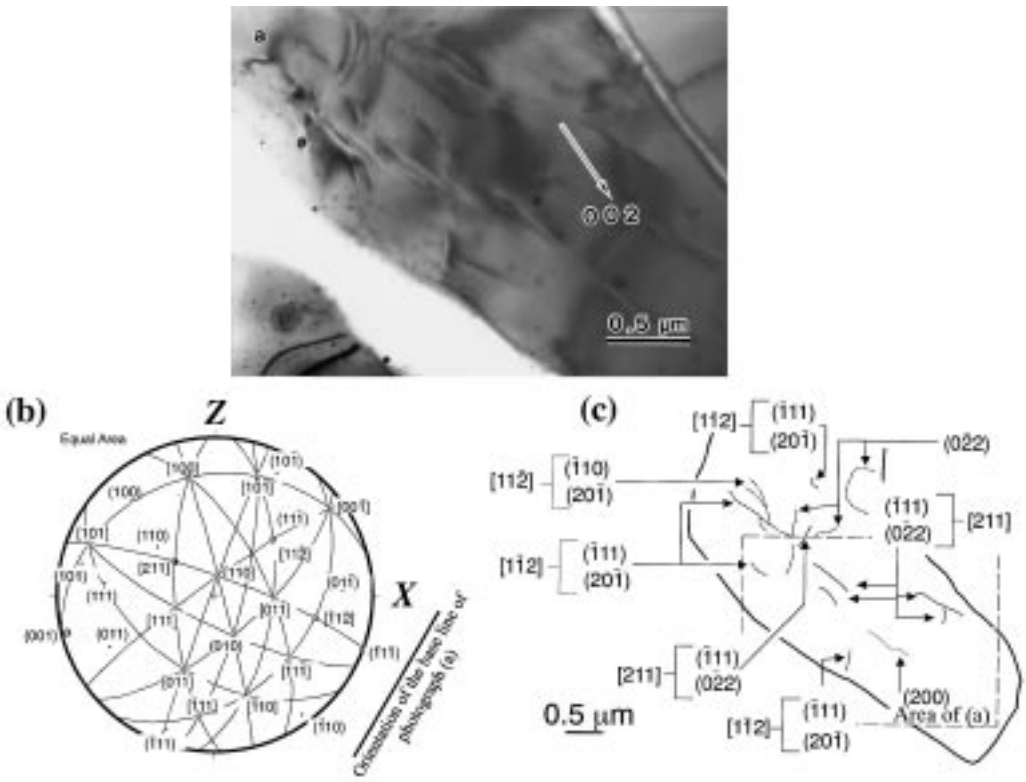

Fig. 10. Substructures in grain II-51. (a) TEM micrographs are taken under the reflections, $\mathbf{g} = (002)$. (b) Crystallographic orientation of grain II-51. (c) Line drawing of dislocations in grain II-51. Diffraction conditions are also shown for which the arrowed dislocations are out of contrast indicated by two or more reflective planes. Burgers vector consistent with this invisibility are also shown. Dislocations with no constraints are not shown.

softening process during the formation of the shear zone, as pointed out by Tullis and Yund (1985) and Tullis et al. (1990).

5.2. Implication of the slip system transition

The plagioclase LPO in this study (Fig. 5) is different from most previous reports (Jensen and Starkey, 1985; Olsen and Kohlstedt, 1985; Kruhl, 1987; Olsen, 1987; Ji and Mainprice, 1988, 1990; Ji et al., 1988, 1994). Only Wenk et al. (1986) and Kruhl (1987) have reported the same LPO patterns as this study. In most of the previously reported LPOs, the (010) pole figure has one point maximum almost parallel to the specimen Z, and the (001) pole figure consists of a single girdle almost parallel to the foliation. In these studies, plagioclase displays abundant optical evidence of plastic deformation such as elongated ribbon-shaped grains, tapered deformation twins, undulatory extinction, and subgrains. These plagioclase samples were deformed under granulite or upper amphibolite facies conditions, and the deformation is mainly controlled by the slip system (010)[001], (Gandais and Williaime, 1984; Olsen and Kohlstedt, 1984, 1985; Montardi and Mainprice, 1987; Ji and Mainprice, 1988). In this study, the TEM observations indicate that the LPO was affected by dislocation glide. However, the slip systems of these dislocations are not (010)[001], but the simultaneous activity of multiple systems, such as dislocations with $\mathbf{b} = 1/2[110]$, $1/2[01\bar{1}]$, $1/2[211]$, $1/2[1\bar{1}2]$, and $1/2[11\bar{2}]$. The microstructures of feldspar are also different from previous studies. The feldspar porphyroclasts display little plastic deformation and exhibit evidence of brittle fracturing (Fig. 2b).

Feldspar deformation is strongly dependent on the deformation conditions (e.g. Simpson, 1985; Tullis and Yund, 1987, 1992; Fitz Gerald and Stünitz, 1993). In experiments (at $\dot{\varepsilon} = 10^{-6}$ s^{-1}), the deformation mechanism changes from brittle fracturing or cataclastic flow ($T < 600^{\circ}$C) to recrystallization-accommodated dislocation creep ($T \geq 900^{\circ}$C) with increasing temperature (Tullis and Yund, 1987, 1992). At higher temperature ($T \geq 1200^{\circ}$C) TEM shows some evidence of dislocation climb. Therefore the difference in the microstructures from previous studies represents the difference in the deformation conditions. This suggests a transition of dominant slip systems from (010)[001] to other slip systems depending on the deformation conditions, as has been proposed for quartz (e.g. Lister and Paterson, 1979; Lister and Hobbs, 1980; Hobbs, 1985; Price, 1985) or olivine (Carter and Avé Lallement, 1970; Mainprice and Nicolas, 1989).

The chemical composition of fine-grained feldspars yielded temperatures of between 330 and 350°C by two feldspar thermometers (Stormer, 1975), although the mineral composition does not significantly change during progressive deformation. However, this temperature is too low to apply the thermometer. On the other hand, the orthoclase mole fraction of the fine-grained alkali-feldspar is restricted to above 0.94. A miscibility gap exists in the $NaAlSi_3O_8$–$KAlSi_3O_8$ system, which depends on the temperature (e.g. Yund and Tullis, 1983). An orthoclase mole fraction above 0.94 is expected at temperatures below 500°C, although the position of the alkali feldspar solvus is controlled by many factors other than temperature, such as coherency and pressure. Therefore, it is concluded that the studied shear zone deformed under much lower temperature (below 500°C) compared with those of previously studied plagioclase deformation. From this, it is inferred that temperature mainly controls the transition of the dominant slip systems from (010)[001].

6. Conclusions

1. The present study provides evidence for deformation by recrystallization-accommodated dislocation creep for fine-grained plagioclase in the ultramylonite. The evidence for dislocation creep is as follows.
   1.1. LPO analyses of the fine-grained plagioclase reveal a strong preferred orientation.
   1.2. Half of the grains can be classified into three orientation groups, *A*, *B*, and *C*. A consistency of the orientation groups with the determined Burgers vectors was found. This indicates the LPO pattern in this study is controlled by dislocation glide.
   1.3. The fine plagioclase grains in the ultramylonite have a variable dislocation density and they have an LPO. These features suggest deformation by recrystallization-accommodated dislocation creep.
2. The LPO pattern presented here is different from those previously reported. From the TEM observations, the dominant slip systems of dislocations are also different from that previously reported (010)[001]. Therefore transition of the dominant slip systems from (010)[001] depending on the deformation conditions is expected, as has been proposed for quartz or olivine.
3. The orthoclase mole fraction of the fine-grained alkali-feldspar suggests that the studied shear zone deformed under the temperature below 500°C, probably under greenschist facies. On the other hand, the plagioclase from most of the previous studies was deformed under amphibolite or granulite facies conditions. Therefore, it is inferred that the temperature controls the transition of the dominant slip systems from (010)[001]. The microstructure of feldspar porphyroclasts also supports this.

Acknowledgements

The authors gratefully acknowledge helpful and constructive discussions with Prof. Mitsuhiro Toriumi and Prof. Toru Takeshita. The authors sincerely thank Prof. Tokuhei Tagai and Prof. Takashi Murakami for their help with the simulation of the theoretical diffraction patterns for $C\bar{1}$ plagioclase by the software Mac Tempus, and Prof. Hideo Takagi and Dr. Christopher A. J. Wibberley for their critical reading of the manuscript. The authors also thank Prof. J. Tullis and an anonymous reviewer for helpful and constructive reviews. The TEM analyses were performed at University of Tokyo with the help of Prof. Toshihiro Kogure and Osamu Tachikawa. The XTG analyses were performed at Ehime University with the help of Prof. Masayuki Komatsu. This research was partially supported by grant-in-aid for Scientific Research from the Ministry of Education of Japan (No. 05402023; Prof. Toshihiko Shimamoto).

References

Allison, I., Barnett, R.L., Kerrich, R., 1979. Superplastic flow and changes in crystal chemistry of feldspars. Tectonophysics 53, 41–46.

Behrman, J.H., Mainprice, D., 1987. Deformation mechanisms in a high-temperature quartz–feldspar mylonite: evidence for superplastic flow in the lower continental crust. Tectonophysics 140, 297–305.

Boullier, A.M., Gueguen, Y., 1975. *SP*-mylonites. Origin of some mylonites by superplastic flow. Contributions to Mineralogy and Petrology 50, 93–104.

Carter, N.L., Avé Lallement, H.G., 1970. High temperature flow of dunite and peridotite. Geological Society of America Bulletin 81, 2181–2202.

Carter, N.L., Tsenn, M.C., 1987. Flow properties of continental lithosphere. Tectonophysics 136, 27–63.

Dell'Angelo, L.N., Tullis, J., 1996. Textural and mechanical evolution with progressive strain in experimentally deformed aplite. Tectonophysics 256, 57–82.

Fitz Gerald, J.D., Stünitz, H., 1993. Deformation of granitoids at low metamorphic grade. I: Reactions and grain size reduction. Tectonophysics 221, 269–297.

Fitz Gerald, J.D., Etheridge, M.A., Vernon, R.H., 1983. Dynamic recrystallization in a naturally deformed albite. Texture and Microstructures 5, 219–237.

Fliervoet, T.F., White, S.H., Drury, M.R., 1997. Evidence for domi-

nant grain-boundary sliding deformation in greenschist- and amphibolite-grade polymineralic ultramylonite from the Redbank Deformed Zone, central Australia. Journal of Structural Geology 19, 1495–1520.

Gandais, M., Williaime, C., 1984. Mechanical properties of feldspars. In: Brown, W.L. (Ed.), Feldspars and Feldspathoids: Structures, Properties and Occurrences, NATO ASI Series. D. Reidel, Dordrecht, pp. 207–246.

Gleason, G.C., Tullis, J., Heidelbach, F., 1993. The role of dynamic recrystallization in the development of lattice preferred orientation in experimentally deformed quartz aggregate. Journal of Structural Geology 15, 1145–1168.

Handy, M.R., 1994. Flow laws for rocks containing two non-linear viscous phases: a phenomenological approach. Journal of Structural Geology 16, 287–301.

Herwegh, M., Handy, M.R., 1996. The evolution of high-temperature mylonitic microfabric: evidence from simple shearing of a quartz analogue (norcamphor). Journal of Structural Geology 18, 689–710.

Hobbs, B.E., 1985. The geological significance of microfabric analysis. In: Wenk, H.-R. (Ed.), Preferred Orientation in Deformed Metals and Rocks: An Introduction to Modern Texture Analysis. Academic Press, Orlando, pp. 463–484.

Jaoul, O., Tullis, J., Kronenberg, A., 1984. The effect of varying water contents on the creep behavior of Heavitree quartzite. Journal of Geophysical Research 89, 4298–4312.

Jensen, L.N., Starkey, J., 1985. Plagioclase microfabrics in a ductile shear zone from the Jotun Nappe, Norway. Journal of Structural Geology 7, 527–539.

Ji, S., Mainprice, D., 1988. Natural deformation fabrics of plagioclase: implications for slip systems and seismic anisotropy. Tectonophysics 147, 145–163.

Ji, S., Mainprice, D., 1990. Recrystallization and fabric development in plagioclase. Journal of Geology 98, 65–79.

Ji, S., Mainprice, D., Boudier, F., 1988. Sense of shear in high-temperature movement zones from the fabric asymmetry of plagioclase feldspars. Journal of Structural Geology 10, 73–81.

Ji, S., Zhao, X., Zhao, P., 1994. On the measurement of plagioclase lattice preferred orientations. Journal of Structural Geology 16, 1711–1718.

Kerrich, R., Allison, I., Barnett, R.L., Moss, S., Starken, J., 1980. Microstructural and chemical transformations accompanying deformation of granite in shear zone at Miéville, Switzerland; with implications for stress corrosion cracking and superplastic flow. Contributions to Mineralogy and Petrology 73, 221–242.

Koshiya, S., 1988. Quartz *c*-axis fabric and microstructure in mylonite—An application to the Hatakawa shear zone. Journal of the Tectonic Research Group of Japan 33, 13–32 (in Japanese with English abstract).

Kronenberg, A.K., Tullis, J., 1984. Flow strengths of quartz aggregates: grain size and pressure effects due to hydrolytic weakening. Journal of Geophysical Research 89, 4281–4297.

Kruhl, J., 1987. Preferred lattice orientations of plagioclase from amphibolite and greenschist facies rock near the Insubric Line (Western Alps). Tectonophysics 135, 233–242.

Kubo, K., Takagi, H., 1997. New finding of pseudotachylyte from the Abukuma granite on the west of Hatagawa fracture zone. Journal of the Geological Society of Japan 103, 798–801 (in Japanese with English abstract).

Kubo, K., Yamamoto, T., 1990. Cretaceous intrusive rocks of Haramachi district, eastern margin of Abukuma Mountains—Petrography and K–Ar age. Journal of the Geological Society of Japan 96, 731–743 (in Japanese with English abstract).

Lister, G.L., Hobbs, B.E., 1980. The simulation of fabric development during plastic deformation and its application to quartzite: the influence of deformation history. Journal of Structural Geology 2, 335–370.

Lister, G.S., Paterson, M.S., 1979. The simulation of fabric development during plastic deformation and its application to quartzite: fabric transitions. Journal of Structural Geology 1, 99–115.

Mainprice, D., Nicolas, A., 1989. Development of shape and lattice preferred orientations: application to the seismic anisotropy of the lower crust. Journal of Structural Geology 11, 175–189.

McLaren, A.C., 1991. Transmission Electron Microscopy of Minerals and Rocks. Cambridge University Press, Cambridge.

Montardi, Y., Mainprice, D., 1987. A transmission electron microscopic study of natural plastic deformation of calcic plagioclase (An 68–70). Bulletin of Mineralogy 110, 1–14.

Olsen, N.Ø., 1987. Plagioclase fabric development in a high-grade shear zone, Jotunheimen, Norway. Tectonophysics 142, 291–308.

Olsen, T.S., Kohlstedt, D.L., 1984. Analysis of dislocation in some naturally deformed plagioclase feldspar. Physics and Chemistry of Minerals 11, 153–160.

Olsen, T.S., Kohlstedt, D.L., 1985. Natural deformation and recrystallization of some intermediate plagioclase feldspars. Tectonophysics 111, 107–131.

Ord, A., Hobbs, B.E., 1989. The strength of the continental crust, detachment zones and the development of plastic instabilities. Tectonophysics 158, 269–289.

Otsuki, K., Ehiro, M., 1992. Cretaceous left-lateral faulting in Northeast Japan and its bearing on the origin of geologic structure of Japan. Journal of the Geological Society of Japan 98, 1097–1112 (in Japanese with English abstract).

Passchier, C.W., Simpson, C., 1986. Porphyroclast systems as kinematic indicators. Journal of Structural Geology 8, 831–843.

Passchier, C.W., Trouw, R.A.J., 1996. Microtectonics. Springer-Verlag, Berlin.

Price, G.P., 1985. Preferred orientation in quartzites. In: Wenk, H.-R. (Ed.), Preferred Orientation in Deformed Metals and Rocks: An Introduction to Modern Texture Analysis. Academic Press, Orlando, pp. 385–406.

Sakai, T., Jonas, J.J., 1984. Dynamic recrystallization: Mechanical and microstructural considerations. Acta Metallurgica 32, 189–209.

Sakai, T., Nagao, Y., Ohashi, M., Jonas, J.J., 1986. Flow stress and substructural change during transient dynamic recrystallization of nickel. Material Science and Technology 2, 659–665.

Sendo, T., 1958. On the granitic rocks of Mt. Otakine and its adjacent districts in the Abukuma massif, Japan. Science Reports of the Tohoku University Third Series 6, 57–167.

Shelton, G.L., Tullis, J., 1981. Experimental flow laws for crustal rocks. Eos Transactions, American Geophysical Union 62, 396.

Shigematsu, N., 1999. Dynamic recrystallization in deformed plagioclase during progressive shear deformation. Tectonophysics 305, 437–452.

Simpson, C., 1985. Deformation of granitic rocks across the brittle–ductile transition. Journal of Structural Geology 7, 503–511.

Stormer, J.C., 1975. A practical geothermometer. American Mineralogist 60, 674–677.

Stünitz, H., 1998. Syndeformational recrystallization—dynamic or compositionally induced? . Contributions to Mineralogy and Petrology 131, 219–236.

Stünitz, H., Fitz Gerald, J.D., 1993. Deformation of granitoids at low metamorphic grade. II: Granular flow in albite-rich mylonites. Tectonophysics 221, 299–324.

Tullis, J., Yund, R.A., 1985. Dynamic recrystallization of feldspar: a mechanism for ductile shear zone formation. Geology 13, 238–241.

Tullis, J., Yund, R.A., 1987. Transition from cataclastic flow to dislocation creep of feldspar: Mechanisms and microstructures. Geology 15, 606–609.

Tullis, J., Yund, R.A., 1991. Diffusion creep in feldspar aggregates: experimental evidence. Journal of Structural Geology 13, 987–1000.

Tullis, J., Yund, R.A., 1992. The brittle–ductile transition in feldspar aggregates: An experimental study. In: Evans, B., Wong, T.-F. (Eds.), Fault Mechanisms and Transport Properties of Rocks. Academic Press, New York, pp. 89–118.

Tullis, J., Dell'Angelo, L., Yund, R.A., 1990. Ductile shear zone from brittle precursors in feldspathic rocks: the role of dynamic recrystallization. In: Duba, A.G., Durham, W.B., Handin, J.W., Wang, H.F. (Eds.), The Brittle–Ductile Transition in Rocks, Geophysical Monograph 56. AGU, Washington, DC, pp. 67–82.

Vernon, R.H., Flood, R.H., 1988. Contrasting deformation of S- and I-type granitoids in the Lachlan Fold Belt, eastern Australia. Tectonophysics 147, 127–143.

Watanabe, I., Sotozaki, Y., Gorai, M., 1953. Geology of the north-eastern border district of northern Abukuma plateau. Science Reports of the Tokyo Education University 2, 69–78 (in Japanese with English abstract).

Wenk, H.-R., 1985. Measurement of pole figures. In: Wenk, H.-R. (Ed.), Preferred Orientation in Deformed Metals and Rocks: An Introduction to Modern Texture Analysis. Academic Press, Orlando, pp. 11–47.

Wenk, H.-R., Pannetier, J., 1990. Texture development in deformed granodiorites from the Santa Rosa mylonite zone, southern California. Journal of Structural Geology 12, 177–184.

Wenk, H.-R., Bunge, H.J., Jansen, E., Pannetier, J., 1986. Preferred orientation of plagioclase-neutron diffraction and U-stage data. Tectonophysics 126, 271–284.

White, S., 1976. The effects of strain on the microstructures, fabrics, and deformation mechanisms in quartzites. Philosophical Transactions of the Royal Society of London A283, 69–86.

Yund, R.A., Tullis, J., 1983. Subsolidus phase relations in the alkali feldspars with emphasis on coherent phases. In: Wenk, P.H. (Ed.), Reviews in Mineralogy: Feldspar Mineralogy. The Mineralogical Society of America, Washington, DC, pp. 141–176.

Yund, R.A., Tullis, J., 1991. Compositional changes of minerals associated with dynamic recrystallization. Contributions to Mineralogy and Petrology 108, 346–355.